Proximity of Acetate, Manganese, and Exchangeable Deuterons to Tyrosine $Y_Z^\bullet$ in Acetate-Inhibited Photosystem II Membranes: Implications for the Direct Involvement of $Y_Z^\bullet$ in Water-Splitting[†]

Dee Ann Force, David W. Randall, and R. David Britt*

Department of Chemistry, University of California, Davis, Davis, California 95616

Received May 28, 1997; Revised Manuscript Received July 16, 1997[⊗]

ABSTRACT: The environment of the photosystem II $Y_Z^\bullet$ radical, trapped in the "split-signal" form, is examined in acetate-treated PSII membranes using pulsed EPR methods. The split-signal line shape is simulated with dipolar and exchange couplings to the Mn cluster of 1260 and −28 MHz, respectively. The 1260-MHz dipolar coupling corresponds to a Mn−$Y_Z^\bullet$ distance of 3.5 Å in the point dipole limit. A 0.117-MHz dipolar coupling is observed between nonexchangeable deuterons of methyl-deuterated acetate and $Y_Z^\bullet$. This interaction is modeled with a 3.1-Å distance between an acetate methyl group deuteron and the phenoxy oxygen of $Y_Z^\bullet$. Since acetate inhibition is competitive with Cl^-, this result strongly suggests a close proximity between $Y_Z^\bullet$ and the Cl^- cofactor binding site. Analysis of pulsed ENDOR and ESEEM experiments investigating the proximity of deuterons exchanged into the vicinity of $Y_Z^\bullet$ after incubation in ^2H_2O-enriched buffer demonstrates that $Y_Z^\bullet$ trapped in the split-signal form participates in two hydrogen-bonding interactions, in contrast to $Y_D^\bullet$, which forms a single hydrogen bond. This result is inconsistent with a simple electron transfer role for $Y_Z^\bullet$ and provides direct experimental evidence for a role for $Y_Z^\bullet$ in proton or hydrogen atom transfer.

Photosystem II (PSII)[1] couples photooxidation of the chlorophyll species P_{680} to the cyclic oxidation of water to molecular oxygen (*1*−*6*). The water oxidation chemistry occurs in an oxygen-evolving complex (OEC), consisting of a tetranuclear manganese cluster, essential cofactors Ca^{2+} and Cl^-, and the redox-active tyrosine Y_Z (D1-Tyr161, *Synechocystis* notation). The oxygen evolution cycle (*7*) involves five "*S*" states, S_0−S_4, where the subscript represents the number of electron equivalents removed from the OEC, referenced to the most reduced state, S_0. Molecular oxygen is released following the formation of the final S_4 state, and the OEC then resets to the S_0 state.

Recent models have invoked the redox-active tyrosine Y_Z directly in the water-splitting chemistry (*6*, *8*−*11*). In these models, the neutral $Y_Z^\bullet$ tyrosine radical, present as an oxidized electron transfer intermediate between P_{680}^+ and the Mn cluster, acts to abstract protons (*8*) or hydrogen atoms (*9*) from substrate water molecules bound to the Mn cluster. A requirement for these models to be correct is a close proximity between Y_Z and water ligands to the Mn cluster, and in part these models were inspired by our previous estimation of a 4.5-Å distance between the Mn cluster and Y_Z in Ca^{2+}-depleted PSII membranes (*8*). A short distance is particularly crucial for the hydrogen atom abstraction model, due to the short tunneling distance possible for the relatively massive hydrogen atom (*12*). On the other hand, the proton abstraction mechanism, which decouples electron transfer from proton transfer, could operate over a longer distance, since electron transfer can take place over a distance of many angstroms, and the proton transfer could involve one or more intermediate proton transfer sites between substrate water and $Y_Z^\bullet$. It is important to further refine our estimate of the distance between Y_Z and the Mn cluster and its substrate water ligands in order to better define possible mechanistic roles for Y_Z in the PSII water-splitting chemistry.

In terms of water accessibility to the Y_Z site, it is clear that in Mn-depleted PSII preparations, deuterons from bulk-phase ^2H_2O can rapidly exchange into the immediate vicinity of $Y_Z^\bullet$, in contrast to deuteron exchange into the $Y_D^\bullet$ site, which is quite slow regardless of the presence or condition of the Mn cluster (*13*, *14*). This is an important result, because exclusion of water from the vicinity of Y_Z would be inconsistent with the predictions of models invoking Y_Z directly in water oxidation. However, since these previous deuteron exchange experiments were performed in Mn-depleted PSII particles, it is not clear how these results relate to water accessibility in the Mn intact system. Unfortunately, due to the rapid Mn → $Y_Z^\bullet$ electron transfer rate in the intact, fully functional OEC, it is not possible to trap $Y_Z^\bullet$ in oxygen-evolving preparations. However, several treatments allow for $Y_Z^\bullet$ trapping in PSII membranes where the Mn cluster is present, albeit in an inhibited form. In such inhibited systems, the $Y_Z^\bullet$ EPR signal is broadened by magnetic interaction with the Mn cluster, resulting in a characteristic split-signal line shape (*8*, *11*, *15*−*20*). The conclusive assignment of the origin of this split-signal to $Y_Z^\bullet$ was provided by ESEEM experiments employing PSII preparations incorporating deuterated tyrosine (*11*).

[†]This work was supported by Grant MCB 9513648 from the National Science Foundation.

* To whom correspondence should be addressed.

[⊗] Abstract published in *Advance ACS Abstracts,* September 15, 1997.

[1] Abbreviations: EPR, electron paramagnetic resonance; CW, continuous wave; OEC, oxygen-evolving complex; PSII, photosystem II; ESE, electron spin echo; ESE-ENDOR, ESE electron nuclear double resonance; ESEEM, ESE envelope modulation; Y_D and Y_Z, D2-Tyr160 and D1-Tyr161, respectively (*Synechocystis* notation); $Y_D^\bullet$ and $Y_Z^\bullet$, neutral radical forms of Y_D and Y_Z, respectively; MES, 2-(*N*-morpholino)ethanesulfonic acid; PPBQ, phenyl-*p*-benzoquinone; Tris, tris(hydroxymethyl)aminomethane; EGTA, ethylene glycol bis(*β*-aminoethyl ether)-*N*,*N*,*N*′,*N*′-tetraacetic acid; DMSO, dimethyl sulfoxide.

S0006-2960(97)01250-6 CCC: $14.00

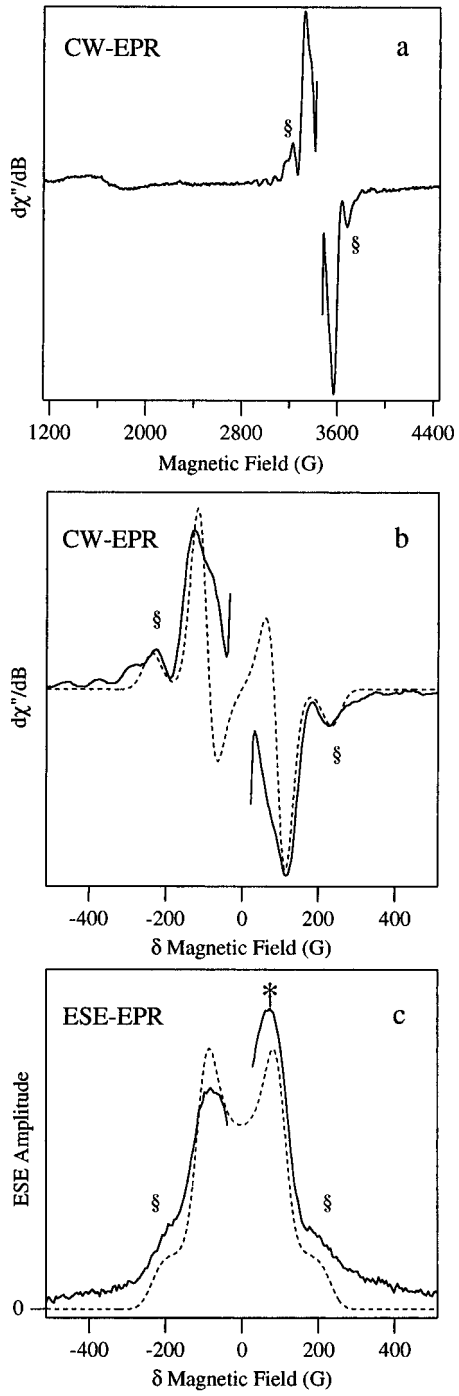

FIGURE 1: Experimental (solid line) and simulated (dashed line) CW derivative EPR spectra (a and b) and ESE absorption EPR spectrum (c) of acetate-treated PSII particles (illuminated minus dark-annealed signals). The large $g = 2$ $Y_D^\bullet$ signal has been excised for clarity. The experimental spectra displayed in panels b and c are plotted as $\delta B = B - B_{g=2}$. Experimental parameters: $\nu_{MW} =$ 9.51 GHz, MW power = 5.1 mW, modulation amplitude = 5 G, modulation frequency = 100 kHz, temperature = 10.0 K (a and b); $\nu_{MW} = 10.013$ GHz; $\tau = 210$ ns; $\pi/2 = 15$ ns, MW power $\approx$ 50 W, repetition rate = 67 Hz, temperature = 4.2 K (c). The simulation was obtained by convolving the experimental spectra with a Pake pattern ($S = 1/2$, $S = 1/2$) with 1260 MHz dipolar and -28 MHz exchange coupling; $r = 3.5$ Å.

Acetate incubation is one treatment that gives rise to the broadened split-signal version of the $Y_Z^\bullet$ radical EPR signal, as displayed in Figure 1a. Acetate appears to inhibit the oxygen evolution chemistry by substituting for the essential Cl^- cofactor (*21*, *22*). The blockage in *S*-state turnover occurs at the S_2-state, allowing one to trap the configuration $S_2 + Y_Z^\bullet$ (*23*, *24*).[2] In such acetate-inhibited PSII membranes, we have examined the accessibility of exchangeable hydrogen sites in the immediate vicinity of $Y_Z^\bullet$ to deuterons introduced from ^2H_2O-enriched buffer using the pulsed EPR methods of electron spin echo−electron nuclear double resonance (ESE-ENDOR) and electron spin echo envelope modulation (ESEEM). ^2H ESE-ENDOR experiments demonstrate the presence of a class of deuteron(s) with hyperfine couplings comparable to that of the well-characterized hydrogen-bonded proton/deuteron site of the dark stable $Y_D^\bullet$ radical. Analysis of the ^2H envelope modulation indicates that there are two such deuterons, in contrast to the case of the ^2H modulation pattern of $Y_D^\bullet$, which arises from a single deuteron. The presence of two such coupled deuterons in close proximity to $Y_Z^\bullet$ provides direct experimental support for the recent models invoking $Y_Z^\bullet$ directly in water oxidation.

In addition, we have performed the ESEEM experiment on PSII samples treated with acetate deuterated at the nonexchangeable methyl group positions ($C^2H_3COO^-$). This experiment probes the distances from $Y_Z^\bullet$ to these ^2H sites, and we model the observed ^2H modulation as arising from an acetate methyl deuteron positioned approximately 3.1 Å from the $Y_Z^\bullet$ phenoxyl oxygen. Given that acetate binds competitively with chloride, this result suggests that the Cl^- cofactor binding site is quite close to $Y_Z^\bullet$. No ^{13}C modulation was observed from preparations incubated with acetate ^{13}C-labeled at either the methyl or the carboxylate carbon. The lack of ^{13}C modulation provides constraints to the orientation of the acetate molecule relative to $Y_Z^\bullet$. In addition, a new analysis of the split-signal line shape in the acetate-treated sample provides an effective dipolar coupling distance of 3.5 Å between $Y_Z^\bullet$ and the Mn cluster. Thus our EPR results lead to a picture of an oxygen evolving complex containing the Mn cluster, the $Y_Z^\bullet$ tyrosine radical, and the cofactor Cl^-, all within very close proximity.

MATERIALS AND METHODS

Materials. ^2H_2O (99.96% deuterium enrichment; low paramagnetic ion content), isotopically-labeled sodium acetates (1-^{13}C, 99% enrichment; 2-^{13}C, 99% enrichment) and isotopically-labeled glacial acetic acids (1-^{13}C, 99% enrichment; 2-^{13}C, 99% enrichment; acetic acid-d_4, 99.5% enrichment) were purchased from Cambridge Isotope Laboratories and used as received. Sodium acetate-d_3 (99% deuterium enrichment) was purchased from ISOTEC and used as received. Phenyl-*p*-benzoquinone (PPBQ) was purchased from Aldrich and recrystallized from an ethanol solution.

Sample Preparation. Oxygen-evolving PSII-enriched membranes were isolated from market spinach using a modification of the method of Berthold *et al.* (*25*−*27*). All steps were performed under coldroom conditions in the dark or under very dim green light. Isolated PSII membranes were resuspended in a storage buffer (400 mM sucrose/20 mM MES−NaOH (pH 6.0)/15 mM NaCl/5 mM $MgCl_2$/5 mM $CaCl_2$) and frozen in liquid N_2. ^2H_2O-exchanged, non-

[2] The split-signal has often been referred to as an S_3-state signal, and indeed it arises from the electron donor side of PSII trapped in a state three oxidation equivalents removed from S_0, but since the origin of the signal has been identified as $Y_Z^\bullet$ interacting magnetically with the Mn cluster in the S_2-state, we prefer the "split-signal" denotation.

acetate-inhibited PSII membranes were resuspended in storage buffer made with ^2H_2O and allowed to incubate in the dark in ice/water with gentle stirring for 12 or 24 h. Control samples in natural abundance ^1H_2O buffer were prepared in a parallel fashion. Acetate-treated PSII membranes (natural abundance, CH_3COO^-; methyl deuterated, $C^2H_3COO^-$; and carboxy carbon labeled, $CH_3{}^{13}COO^-$) were prepared by washing PSII membranes three times in a buffer containing 400 mM sucrose/40 mM MES−NaOH (pH 5.5)/500 mM sodium acetate (SMAc buffer) at sequential concentrations of 0.2, 0.3, and 0.6 mg of Chl/mL, based on the methods of MacLachlan and Nugent (*28*) and Szalai and Brudvig (*23*). The methyl carbon-labeled acetate ($^{13}CH_3COO^-$) samples were washed twice in 400 mM sucrose/40 mM MES−NaOH (pH 5.5) (SM buffer) and once in $^{13}CH_3COO^-$ SMAc buffer; these samples were found to display equivalent split-signal EPR line shapes and amplitudes as the samples prepared with acetate in all three wash steps (data not shown). ^2H_2O-exchanged acetate-treated PSII membranes were prepared by 1.5-, 12-, and 24-h incubations in SMAc buffer (pD 5.5) made with ^2H_2O. All the previously listed buffers were pH[pD] adjusted using the corresponding isotopically-labeled glacial acetic acid.[3] The PSII samples were loaded into 3.8 mm o.d. precision quartz EPR tubes at a concentration of 18−20 mg of Chl/mL in the appropriate buffers with 1 mM PPBQ added (final concentration; from a 200 mM stock solution in DMSO). After 30−45 min of dark adaptation in ice/water, the samples were stored in liquid N_2 until use.

Illumination of the acetate-treated PSII samples in order to generate the split-signal form of the $Y_Z^\bullet$ radical was performed at room temperature for 5 s using a focused 300-W IR-filtered Radiac light source along with a Schott 150-W IR-filtered fiber optic lamp, immediately followed by freezing in liquid N_2. "Annealing" of split-signal samples was performed by incubation in total darkness for 25 min in ice/water before refreezing in liquid N_2. The $Y_D^\bullet$ radical was generated in PSII samples by 1-min illumination in ice/water, followed by a 1-min dark incubation before freezing in liquid N_2.

The ribonucleotide reductase R2 protein samples were provided by Dr. Pamela Riggs-Gelasco and Professor JoAnne Stubbe. These were prepared as described by Salowe and Stubbe (*29*) with modifications as reported in Bollinger *et al*. (*30*). The ^2H_2O-exchanged sample was prepared by an incubation for 5 h in 100 mM HEPES buffer (pH 7.7) prepared in ^2H_2O. This ^2H_2O sample and the parallel ^1H_2O control sample were loaded into EPR tubes at approximately 1 mM protein concentration and stored in liquid N_2 until use.

EPR Spectroscopy. CW-EPR spectra were collected at a temperature of 10.0 K with a Bruker ECS106 X-band CW-EPR spectrometer equipped with an Oxford ESR900 liquid helium cryostat and an ITC503 temperature controller. Field-swept ESE, ESEEM, and ESE-ENDOR spectra were collected at a temperature of 4.2 K with a laboratory-built pulsed EPR spectrometer (*31, 32*). Three-pulse time-domain ESEEM experiments were performed by incrementing the time T in the stimulated echo sequence: $\pi/2-\tau-\pi/2-T-\pi/2-\tau-$stimulated echo (*33, 34*). ESEEM spectra were recorded both following illumination to trap the split-signal and following subsequent annealing to detrap the split-signal. After subtraction of the annealed sample data from the illuminated sample data, the resultant "light-minus-dark" time domain data sets were then normalized in deuterated/natural abundance pairs, and (deuterated/natural abundance) ratioed modulation patterns were generated in order to isolate only those features arising from deuteron exchange (*35*). A cosine Fourier backfill procedure (*36*) was used to reconstruct the instrumental dead time for all three-pulse data in order to generate the final displayed Fourier transforms. Computer simulations of the ESEEM time domain data were based on the density matrix formalism of Mims (*37*) using the numerical algorithm described by Britt *et al*. (*38*). ESE-ENDOR experiments utilized the sequence introduced by Mims (*39*), which employs the stimulated echo sequence with a radio frequency pulse applied during the T interval.

RESULTS

We have previously demonstrated that ^2H ENDOR can provide detailed information about hydrogen bonding to tyrosine radicals (*40*). Couplings to exchangeable hydrogens in the vicinity of the radicals can in principle be measured by subtraction of ^1H ENDOR spectra obtained before and after exchange with ^2H_2O, but the use of ^2H ENDOR alleviates the need for the potentially problematic ^1H ENDOR spectral subtractions and can also give information about the nuclear quadrupole interaction for the $I = 1$ ^2H nucleus. Figure 2 displays the Mims ^2H ESE-ENDOR spectrum obtained for $Y_Z^\bullet$ trapped in the split-signal form in acetate-treated membranes, as well as results for $Y_D^\bullet$, $Y_Z^\bullet$ in a Mn-depleted Y_D-less preparation, and the tyrosine radical of *Escherichia coli* ribonucleotide reductase (RNR). The traces denoted (a) show the ^2H ENDOR obtained for the acetate-treated PSII preparation with the shortest time exposure (≈1.5 h) to ^2H_2O-enriched buffer. The ENDOR spectra were collected at a field position 75 G upfield from the center of the large$Y_D^\bullet$ radical signal, as denoted with an asterisk in the ESE-EPR spectrum of Figure 1c. The ENDOR spectrum ("light") obtained on the split-signal shows a broad bi-lobal ENDOR pattern centered at the ^2H Larmor frequency. After annealing the sample in the dark to detrap the $Y_Z^\bullet$ radical giving rise to the split-signal, the ^2H ENDOR spectrum ("dark") is essentially flat in the region around the ^2H Larmor frequency, demonstrating that the observed features indeed arise from the trapped $Y_Z^\bullet$ radical. The overall width of the ^2H ENDOR powder pattern is quite comparable to that of the dark stable$Y_D^\bullet$ radical (trace b) measured in spinach PSII preparations following 24 h ^2H_2O exchange (*40*). We have recently demonstrated in PSII particles from *Synechocystis* that the hydrogen bond donor to$Y_D^\bullet$ is the D2-His189 τ nitrogen (*41*). In spinach PSII, the distance between the phenoxyl oxygen and the hydrogen-bonded $^1H(^2H)$ provided by the analogous histidine nitrogen (His190) is approximately 1.81 Å.[4] The breadth of the ^2H ENDOR pattern in trace (a) provides convincing evidence that $Y_Z^\bullet$ trapped in the split-signal form in acetate-treated PSII membranes is also hydrogen bonded. The major spectral difference between the split-signal spectrum (trace a) and the $Y_D^\bullet$ spectrum (trace b) is that ^2H ($I = 1$) quadrupolar doublets are not resolved

[3] ESEEM of acetate-treated samples prepared in 40 mM ^2H_2O buffer, supplying an exchangeable ^2H concentration higher than that provided by the $C^2H_3COO^2H$ glacial acetic acid used for pD adjustment, showed no detectable ^2H modulation.

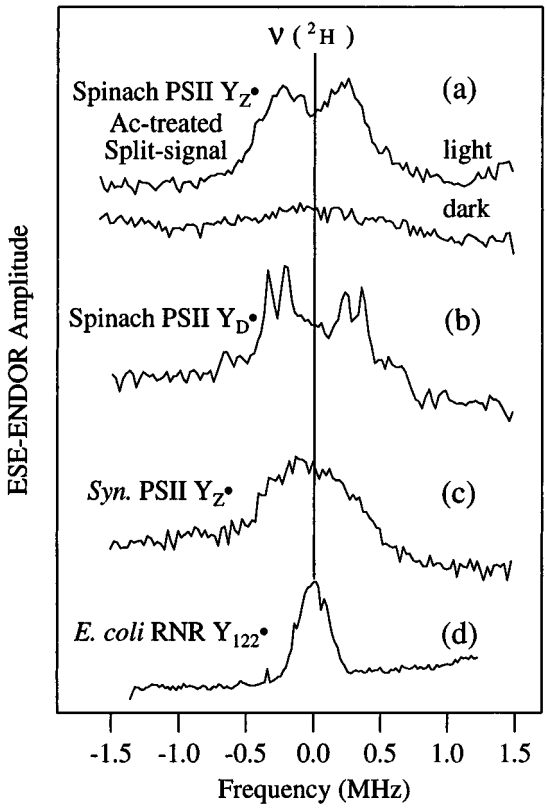

FIGURE 2: Mims ^{2}H ESE-ENDOR spectra of tyrosine radicals. (a) Spectra from illuminated (light) and dark-annealed (dark) acetate-treated spinach PSII membranes incubated for 1.5 h in ^2H_2O buffer. (b) Spectrum of $Y_D^\bullet$ in Tris-washed Mn-depleted spinach PSII membranes incubated for 3 h in ^2H_2O buffer (adapted from ref 40). (c) Spectrum of $Y_Z^\bullet$ in a Mn-depleted *Synechocystis* PSII core preparation from a Y_D-less mutant (D2-Tyr160Phe) incubated in ^2H_2O as in panel b (adapted from ref 40). (d) Spectrum of Y_{122} in *E. coli* ribonucleotide reductase incubated for 5 h in ^2H_2O buffer. Spectra are plotted as $\delta\nu = \nu_{RF} - \nu_{^2H}$; $\nu_{^2H} = 2.38$ MHz at $B =$ 3650 G (a). Experimental parameters: $\nu_{MW} = 10.013$ GHz (a), 10.103 GHz (b), 10.106 GHz (c), 10.109 GHz (d); B 3650 G (a), 3603 G (b), 3609 G (c), 3618 G (d); $\tau = 500$ ns; $\pi/2 = 15$ ns; MW power ≈ 70 W (a), 60 W (b), 40 W (c), 10 W (d); RF pulse = 40 μs; RF power ≈ 0.3 kW (a), 0.1 kW (b and c), 1 kW (d); repetition rate = 333 Hz (a), 25 Hz (b and c), 200 Hz (d); temperature = 4.2 K.

in the former.[5] However the overall splitting pattern is consistent with dipolar coupling between the spin density on the tyrosyl oxygen and one or more hydrogen-bonded ^{2}H nuclei. The spectrum can be compared to the featureless ENDOR pattern observed for $Y_Z^\bullet$ in Mn-depleted Y_D-less *Synechocystis* PSII particles (trace c) (*40*). This structureless ^{2}H ENDOR spectrum has the same overall line width as the split-signal spectrum and the spectrum of $Y_D^\bullet$, indicating that $Y_Z^\bullet$ is hydrogen-bonded even in the Mn-depleted preparation. However, the complete lack of structure indicates that this hydrogen bonding is highly disordered. These PSII tyrosine radical ^{2}H ENDOR line width can be contrasted to the much narrower ^{2}H ENDOR line widths observed for the *E. coli* ribonucleotide reductase tyrosine ($Y_{122}^\bullet$, trace d), a tyrosine radical in which hydrogen bonding appears to be absent (*45*).

The ESE-ENDOR technique provides for high-resolution spectra of magnetically coupled deuterons, but it is difficult to determine the number of nuclei contributing to the spectra. Conversely, the modulation depth of ESEEM patterns contains quantitative information about numbers of proximal nuclear spins, though the spectral resolution may be poor because the frequency domain ESEEM powder patterns of dipolar coupled nuclei have zero intensity at the canonical parallel and perpendicular turning points (*46*). However, the *combination* of ESEEM and ESE-ENDOR can provide full characterization of the nuclear spin environment of the tyrosine radicals. Figure 3a displays the ^{2}H/^{1}H ratioed three-pulse time-domain ESEEM spectrum of the 1.5 h ^2H_2O-incubated split-signal sample used in the ^{2}H ENDOR experiments of Figure 2a. Figure 3a′ shows the Fourier transform of the ratioed time-domain spectrum, with a single peak occurring at the 2.38-MHz ^{2}H Larmor frequency. From our previous ESE-ENDOR study (*40*), we know accurate spin Hamiltonian parameters for the class of deuterons coupled to $Y_D^\bullet$ ($A_{iso} = 0$; $T_{dip} = 0.570$ MHz; $e^2qQ = 0.20$ MHz; $\eta = 0$). Since the line shape of the split-signal ^{2}H ENDOR spectrum of Figure 2a is similar, albeit less resolved, we can use these fixed parameters to simulate the ^{2}H ESEEM of the split-signal. The simulation using a single deuteron with these parameters (Figure 3a, upper dashed trace) shows much shallower modulation than observed in the experimental spectrum. Simulations employing one such hydrogen-bonded deuteron supplemented with a number of more weakly-coupled deuterons modeling more distant sites also fail to match the experimental spectrum (data not shown). However, the simulation obtained using *two* deuterons with the spin Hamiltonian parameters of the $Y_D^\bullet$ hydrogen-bonded deuteron provides an excellent simulation of the experimental ESEEM spectrum (Figure 3a, lower dashed trace). This excellent simulation obtained with known hydrogen-bonded tyrosine ^{2}H ENDOR spectral parameters, with no variables other than the number of coupled deuterons, provides very strong evidence that two deuterons exchange into hydrogen-bonding positions about the $Y_Z^\bullet$ radical in the acetate-inhibited PSII membranes. The moderate disorder inherent in the ^{2}H ENDOR of the split-signal may arise from a slight inequivalence in the hyperfine and/or quadrupolar couplings of the two deuterons. However, the inequivalence in the hyperfine coupling must be small, because ESEEM simulations generated by varying the dipolar couplings by more than approximately 15% show a significantly poorer match to the experimental spectrum (not shown). Longer term incubation of the acetate-treated samples in ^2H_2O resulted in slightly deeper ^{2}H modulation, with an increase of approximately 10% following 12- or 24-h ^2H_2O incubation (data not shown). The modulation patterns for the longer exchanged samples cannot be fit as well with a pair of equivalent deuterons, probably because additional, more remote, slowly exchanging sites become deuterated. We

[4] Radial distances between the electron spin and an exchangeable proton or deuteron can be calculated from the dipolar hyperfine couplings used in the expression $T_{dip} = \rho_O g_e g_N \beta_e \beta_N / r^3$, where ρ_O is the unpaired spin density on the tyrosyl oxygen, g_e and β_e are the electronic g-factor and Bohr magneton, and g_N and β_N are the nuclear g-factor and nuclear magneton. In this work, we use the ρ (^{17}O) = 0.28 spin density value recently measured for $Y_D^\bullet$ in ^{17}O-labeled PSII membranes from *Synechocystis* (*42*) to obtain 1.81 Å for the radial distance. It is certainly possible, however, that there are slight species variations in ρ_O, as there are for the spin densities at other tyrosine positions (*43*). However, the literature value currently available for spinach (*43*) is a combined C_4 and tyrosyl oxygen spin density, $\rho_{C_4+O} = 0.22$; to use this number as ρ_O, one must assume $\rho_{C_4} = 0$. In that case, the analogous calculated radial distance is 1.67 Å as previously published (*40*).

[5] The spectral resolution is more comparable to the first hydrogen-bonded ^{2}H Mims ENDOR reported, that observed in *Anabaena ferredoxin* (*44*).

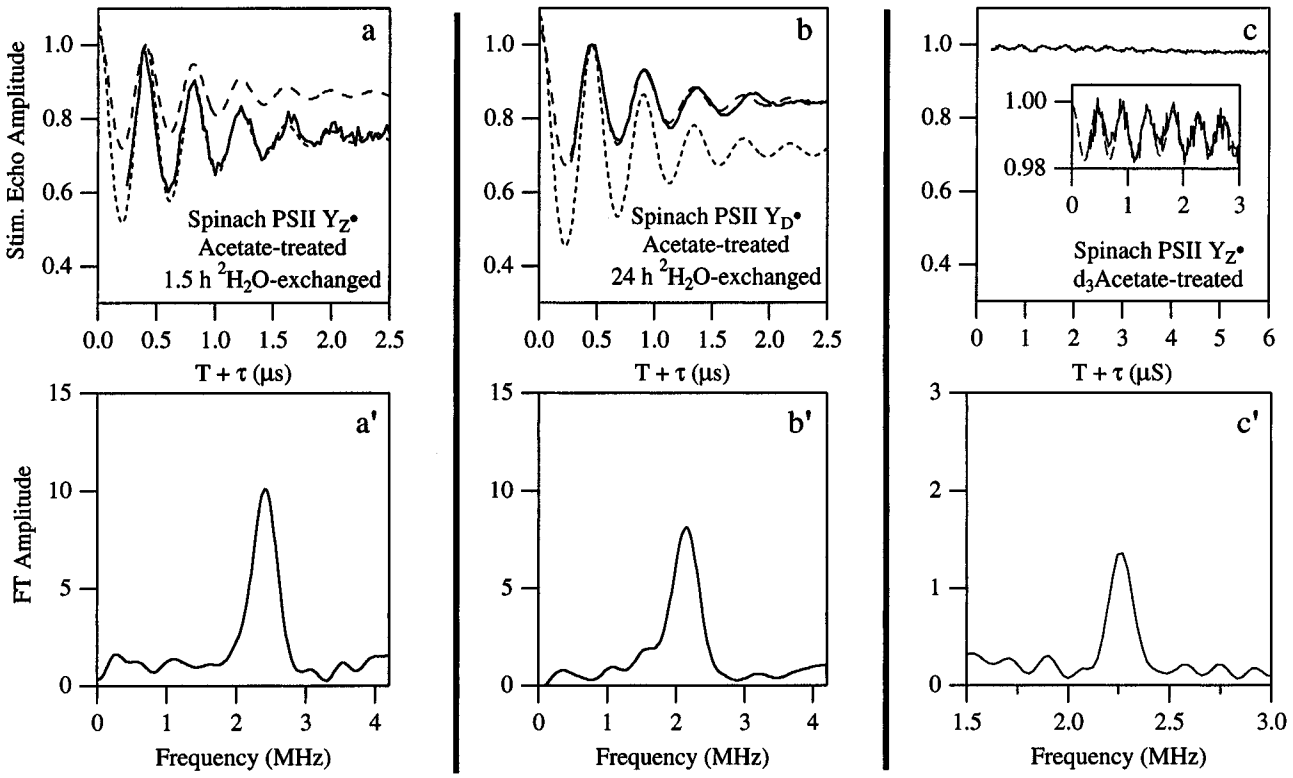

FIGURE 3: Time domain and frequency domain for $^2H/^1H$ ratioed three-pulse ESEEM spectra of the split-signal of acetate-treated PSII membranes incubated for 1.5 h in ^2H_2O buffer (a and a′; illuminated minus dark-annealed signals), $Y_D^•$ in spinach PSII particles incubated for 24 h in ^2H_2O buffer (b and b′), and the split-signal of $C^2H_3COO^-$ acetate-treated PSII membranes (c and c′; illuminated minus dark-annealed signals). Inset c: time domain magnified to show detail. The experimental data are shown as solid lines; the time domain simulations are short dashes for one ^2H (a, b, and c: inset) and long dashes for two ^2H (a and b). Experimental parameters: $\nu_{MW} = 10.013$ GHz (a and a′), 9.203 GHz (b and b′), 9.2594 GHz (c and c′); $B = 3650$ G (a and a′), 3292 G (b and b′), 3385 G (c and c′); $\tau = 210$ ns (a and a′), 214 ns (b and b′), 208 ns (c and c′); starting $T = 65$ ns (a and a′), 66 ns (b and b′), 72 ns (c and c′); $\pi/2 = 15$ ns; MW power ≈ 50 W (a, a′, b, and b′), 13 W (c and c′); repetition rate = 200 Hz (a and a′), 25 Hz (b and b′), 333 Hz (c and c′); temperature = 4.2 K. Simulation parameters: $A_{iso} = 0$; $e^2qQ = 0.20$ MHz; $\eta = 0$; $T_{dip} = 0.570$ MHz (a and b), 0.117 MHz (c).

consider the quickly exchangeable sites, populated by deuterons in the shortest time incubation, to be those most relevant to possible roles of $Y_Z^•$ in OEC substrate water oxidation.

For comparison with the modulation observed for the split-signal, Figure 3 panels b and b′ display the time and frequency domain ESEEM for $Y_D^•$ in spinach PSII membranes incubated for 24 h in ^2H_2O. The time-domain ESEEM pattern is simulated very well using only one deuteron with the ENDOR-determined hyperfine and quadrupolar parameters (Figure 3b, upper dashed trace), consistent with there being only one such hydrogen-bonded deuteron for the $Y_D^•$ tyrosine radical. We have previously argued (*41*) that the excellent simulation of the high-resolution ^2H ENDOR for $Y_D^•$ using a single class of coupled deuteron(s) made it unlikely that there are two hydrogen bond donors to $Y_D^•$; in this case, unless the two deuterons possess extraordinarily equivalent couplings, they would give rise to a spectrum broadened beyond that of the single deuteron spectral simulation (such as the broadening seen in the split-signal spectra in Figure 2a). The excellent simulation of the ESEEM spectrum using a single deuteron with ^2H ENDOR-fixed parameters greatly strengthens the evidence that there is indeed a single hydrogen bond to $Y_D^•$. We observe slightly deeper modulation upon ^2H_2O exchange for times greater than 24 h, but again this additional modulation appears to arise from more distant deuterons than the hydrogen-bonded deuteron that gives the modulation pattern of Figure 3b.

Figure 3, panels c and c′, displays the results of ESEEM experiments utilizing acetate deuterated at the methyl hydrogen positions to probe the accessibility of acetate to the region immediately surrounding $Y_Z^•$. These experiments take advantage of the nonexchangeability of the methyl deuterons: all observed deuteron modulation arises solely from these chemically defined methyl deuterons and not from deuterons exchanged into other sites as in the previously described ^2H_2O incubation experiments. The illuminated-minus-annealed $C^2H_3COO^-/C^1H_3COO^-$ ratioed ESEEM spectrum (trace 3c) shows shallow modulation that corresponds to the Larmor frequency, as seen by the narrow peak at 2.26 MHz in the Fourier transform (trace c′).[6] The shallow modulation dampens extremely slowly (Figure 3c and inset). The dashed line superimposed on the inset trace illustrates a simulation for a single ^2H with a dipolar coupling of 0.117 MHz. If we consider this coupling to arise from an interaction with the spin density on the tyrosine oxygen (the same assumption used in the hydrogen bond distance calculations), this coupling corresponds to a ^2H-O distance of 3.1 Å. Because of the $1/r^6$ distance dependence on modulation depth of weakly-coupled ESEEM, the distance only increases to 3.7 Å if we assume that all three methyl deuterons are (equivalently) coupled to $Y_Z^•$. We also

[6] There is also ^2H modulation in the background signal, so it is important to obtain accurate light-minus-dark difference spectra. Identical difference spectra were obtained for two independent sets of samples and pulsed EPR runs.

performed analogous ESE-ENDOR and ESEEM experiments on samples treated with acetate ^{13}C-labeled alternatively at the methyl and carboxylate carbons. No ^{13}C couplings to $Y_Z^\bullet$ trapped in the split-signal form were observed.[7]

DISCUSSION

EPR Line Shapes. We have previously (*8*) estimated a distance of 4.5 Å from $Y_Z^\bullet$ to the Mn cluster in Ca^{2+}-depleted PSII membranes. This distance came from the assumptions that the coupling is dipolar in nature and that the Mn cluster is in an EPR silent integral spin $S = 1$ state. The split-signal generated in acetate-treated membranes (Figure 1) is somewhat broader than that of Ca^{2+}-depleted membranes. Szalai and Brudvig (*24*) have presented clear evidence that the Mn cluster is in the S_2-state when the split-signal is present. In fact, after quenching this $Y_Z^\bullet$ signal with NO, the familiar multiline signal reappears (*24*). Moreover, the acetate-inhibited form of the split-signal has a conspicuous set of flanking features (marked with § in Figure 1) in the field range past the principal split peaks. These satellite peaks have amplitudes well above the peak heights of the small underlying multiline signal.[8] It is clearly not possible for this additional structure to arise from an $S = 1/2$ Mn cluster state broadening the $Y_Z^\bullet$ signal through a purely isotropic exchange interaction. However, if the coupling contains a considerable dipolar component, the principal "split" peaks could correspond to the perpendicular turning points of the overall Pake powder pattern, and the satellite peaks could correspond to the parallel turning points. The dashed lines of Figure 1, panels b and c, are simulations to both the CW and ESE EPR spectra based on such an assignment. The spectral features are very well simulated with a relatively large dipolar coupling of 1260 MHz and a smaller exchange interaction of −28 MHz. In the limit of a point dipole approximation, this dipolar coupling corresponds to a Mn−$Y_Z^\bullet$ distance of only 3.5 Å. This would appear to place the Mn cluster sufficiently close to $Y_Z^\bullet$ to allow direct H atom transfer from water ligands of the cluster to $Y_Z^\bullet$.[9]

It is clear in our light-minus-annealed ESE spectra (Figure 1c) that there is no multiline signal of appreciable intensity that disappears upon annealing. This is consistent with our results on the Ca^{2+}-depleted form (*8*), in which the split-signal was not observed to rise atop an ESE-detected dark-stable multiline signal (*20, 52*). That work was in conflict with results reported by Zimmermann *et al.* (*53*), who reported that the multiline signal is detectable along with the split-signal in ESE-EPR. In the case of the acetate treatment, there is no "dark-stable" multiline, so any ESE-detectable multiline signal should disappear during the 25-min annealing step. We see no evidence of such changes, indicating that no significant multiline signal is detectable by ESE (or CW-EPR) spectroscopy from those S_2-state clusters coupled to $Y_Z^\bullet$.

It is interesting to consider why no appreciable multiline EPR signal is detected in the presence of $Y_Z^\bullet$. After all, with a paramagnetic tetranuclear metal cluster close by, the $Y_Z^\bullet$ radical can still be detected, albeit with broadened line shape. It is clearly not possible that this same Mn−$Y_Z^\bullet$ coupling, viewed from the perspective of the Mn cluster, could broaden a readily-detectable ESE spectrum with a 600-G line width (full width at half maximum peak height) sufficiently to lead to its disappearence. Simulations utilizing the same electron−electron coupling and spectral broadening that provide the good split signal simulation (Figure 1, panels b and c) do show a loss of resolved ^{55}Mn hyperfine features, but the increase in the overall line width of the multiline field-swept ESE spectrum is negligible (simulation not shown). We therefore suggest as an alternative explanation that the lack of observed multiline signal in centers with $Y_Z^\bullet$ trapped is not caused directly by the $Y_Z^\bullet$−Mn magnetic interaction, but by a change in the couplings *within* the tetranuclear Mn cluster caused by a perturbation of its environment when the proximal Y_Z tyrosine is oxidized and deprotonated. For example, Szalai and Brudvig (*24*) have demonstrated that in the acetate-treated membranes, the $g = 4.1$ EPR signal form ($S = 5/2$ or possibly 3/2) of the S_2-state Mn cluster is initially formed, but that the $S = 1/2$ multiline signal form is observed when the diamagnetic NO−$Y_Z^\bullet$ adduct is created. This clearly demonstrates that chemical changes at the adjacent Y_Z tyrosine affect the internal couplings within the Mn cluster. Perhaps when Y_Z is oxidized to $Y_Z^\bullet$, the phenolic proton is transferred to a ligand or bridging group of the cluster, affecting the internal couplings. In any event, the change of internal coupling could alter the ground spin state of the cluster, rendering it effectively EPR silent. Although the $S > 1/2$ $g = 4.1$ signal is indeed EPR detectable, another $S > 1/2$ state with a different set of zero-field splitting parameters and possible dispersion of these parameters could have such a broad magnetic field distribution of signal intensity so as not to be observable.[10] Alternatively, the ground state of the S_2-state of the cluster could be $S = 1/2$, but changes in the intercluster interactions could lead to very low-lying excited states that provide ultrafast relaxation via the Orbach process (*54*−*56*)

[7] No ^{13}C couplings were observed in the ESEEM for either illuminated or annealed samples. ^{13}C ENDOR peaks were observed for both labeled carbons, but within the signal-to-noise level these were identical between illuminated and annealed samples, so we cannot assign these features to ^{13}C nuclei coupled to $Y_Z^\bullet$.

[8] The underlying multiline signal is ≈6% the size of a control multiline signal generated by 200K illumination of untreated PSII membranes.

[9] The simulations in Figure 1 utilized Pake patterns which pairwise cross over the $g = 2$ region, i.e. the parallel features at ±200 G are associated with the perpendicular features at ∓100 G. The alternative assignment, with parallel features at ±200 G associated with perpendicular features at ±100 G, gives a much poorer simulation (not shown). Such an alternative simulation predicts an exchange coupling of 330 MHz and a dipolar coupling of 680 MHz, with a corresponding point dipole distance of 4.3 Å. In our analysis of proton ENDOR and deuteron ESEEM spectra of the PSII Mn cluster and relevant model compounds, we are currently addressing the modifications needed to go beyond the simple single-point dipole approximation to calculate $^1H/^2H$-Mn distances in multinuclear Mn clusters. For dinuclear clusters, analytic expressions can be developed for the hyperfine tensor components as a function of distance and relative orientation with respect to the two Mn ions, taking into account the appropriate spin projection factors for the two ions in the exchange-coupled representation used to model the ground-state magnetic parameters (*47, 48*). For the tetranuclear clusters, we are utilizing the projection factors that lead to good simulations of the multiline CW EPR (*49*) and ^{55}Mn ENDOR spectra (*50*) along with various proposed structural models for the Mn cluster to numerically calculate the range of possible $^1H/^2H$-Mn distances for a given observed dipolar hyperfine coupling (*51*). The maximum distances calculated in this manner extend 25% beyond the simple single-point dipole approximation distance. The same range of values could equivalently be used in modeling the electron−electron dipolar couplings in this work. Therefore we estimate a distance range of between 3.5 and 4.4 Å using this tetranuclear cluster modeling approach.

Scheme 1

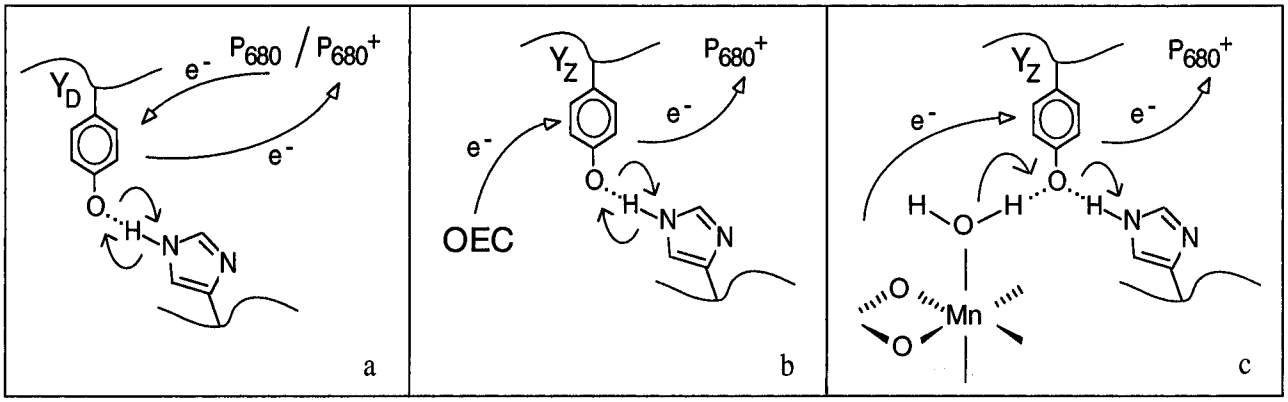

or provide direct interspin-state mixing (*57*). In either case, the presence of the Mn cluster in the S_2-state without an EPR signal is well precedented; no Mn EPR signal is observed after illumination of Cl^--depleted membranes, yet subsequent addition of Cl^- in the dark leads to the formation of the $g = 2$ multiline signal without further illumination (*58*). We would interpret the lack of a Mn EPR signal in the Cl^--depleted preparations in the same context as described above, by which removing the essential Cl^-, possibly as a ligand to the cluster, alters the intracluster couplings in such a way that renders the paramagnetic Mn cluster effectively EPR silent.

OEC Topology. Our ESEEM study utilizing methyl group deuterated acetate shows that even with the Mn cluster present, the relatively large acetate ion can bind at a site within a few angstoms of $Y_Z^\bullet$. This is certainly contrary to the view that $Y_Z^\bullet$ is buried well away from the aqueous phase, preventing this highly oxidizing species from forming deleterious radicals (*59*). Given the distance constraints from the observed ^2H modulation and the lack of observed ^{13}C modulation, we can extract information about the relative positioning, including orientation, of the acetate ion relative to $Y_Z^\bullet$. Figure 4 displays a possible geometry of the acetate ion relative to $Y_Z^\bullet$, assuming the ^2H modulation arises from a methyl deuteron close to the oxygen of the $Y_Z^\bullet$ phenoxy side chain. This approximation seems appropriate given the unlikelihood that the acetate anion would dock along the hydrophobic ring or methylene group of the tyrosine side chain. Utilizing the $\rho(^{17}O) = 0.28$ value measured for $Y_D^\bullet$ in ^{17}O-labeled *Synechocystis* PSII membranes (*42*), the calculated distance between the acetate methyl ^2H and the $Y_Z^\bullet$ phenoxy O distance is 3.1 Å. Modeling possible $^{13}C-O$ interactions in the same fashion limits the distance from either acetate carbon to the tyrosyl oxygen to greater than 3.6 Å.[11] In the geometry displayed in Figure 4, with the methyl group of acetate positioned closest to $Y_Z^\bullet$, the closest

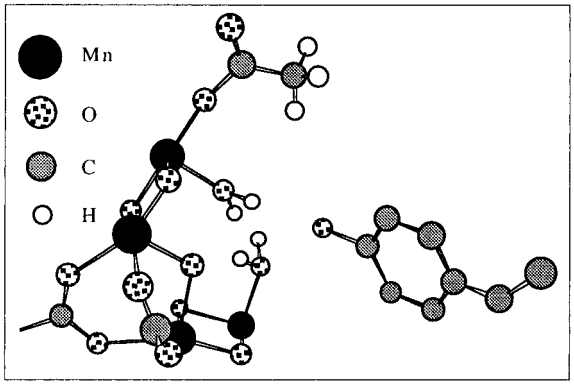

FIGURE 4: Model for the acetate-inhibited OEC, based on our previous structural model (*6*), incorporating the EXAFS-derived tetranuclear cluster model (*5, 60*) into a site proximal to $Y_Z^\bullet$.

carbon is 4.0 Å from the phenoxyl oxygen. The opposite orientation, with the carboxy moiety directed toward $Y_Z^\bullet$, violates the constraint provided by the lack of ^{13}C modulation.

It is appealing, given the similar distances calculated from $Y_Z^\bullet$ to the Mn cluster and to the acetate ion, to also consider the possibility that acetate is bound directly to the Mn cluster. Thus in Figure 4, we also illustrate a possible Mn−acetate binding motif, elaborating on the structural model discussed in our recent O_2 evolution review (*6*). In this OEC model, a tetranuclear Mn cluster (*5, 60*) is shown with terminally-bound waters adjacent to the phenoxyl group of $Y_Z^\bullet$.

Since the acetate ion inhibits oxygen evolution at a chloride-competitive site (*21, 22*), we can infer that $Y_Z^\bullet$ is also in very close proximity to the binding site of the Cl^- cofactor.[12] UV difference spectroscopy has recently shown that Cl^- is required to facilitate the $S_2 \rightarrow S_3$ transition (*61*). Thus when acetate inhibits by replacing Cl^-, the Mn cluster is trapped in the S_2-state, and $Y_Z^\bullet$ can then be trapped in its broadened split-signal form upon further oxidation by P_{680}^+. It has been suggested that Cl^- facilites electron transfer within the Mn cluster by binding directly as a bridging or

[10] The fact that the split-signal is not observed with unity stoichiometry could be a result of a higher-spin state of the Mn cluster if the $Y_Z^\bullet$ signal coupled to $|m_s| > 1/2$ manifolds is broadened beyond detectability due to the greater anisotropy that would result from the larger $|m_s|$ values. For example, if essentially all Y_Z centers are trapped in the $Y_Z^\bullet$ form, but the Mn cluster is in an $S = 3/2$ state, only those tyrosine radical centers coupled to the $|m_s| \pm 1/2$ manifolds would be observed as "split-signal", leading to the maximal 50% integrated area of this signal relative to that of $Y_D^\bullet$ reported by Szalai and Brudvig (*23*). Moreover, in such a model the calculated Mn cluster−Y_Z distance is independent of the specific half-integral S value because the observed split-signal would arise only from the $|m_s| \pm 1/2$ manifolds.

[11] Utilizing the relationship between modulation depth and nuclear spin, we can establish a maximum radial distance between an acetate ^{13}C nucleus and the tyrosyl oxygen that could be detected with ESEEM. Given a modulation depth that is 3/8 smaller for ^{13}C ($I = 1/2$) than ^2H ($I = 1$) and a minimal experimental modulation depth of approximately 0.007 based upon the signal-to-noise ratio of the $^2H/^1H$ ESEEM data [Figure 3c; the noise signature found in the $^{13}C/^{12}C$ ESEEM data (not shown) is essentially the same], we estimate a maximum distance of 3.6 Å for detection of a single weakly-coupled ^{13}C nucleus.

terminal ligand (*61*, *62*). This direct binding model is certainly consistent with our results indicating that both the Mn cluster and the Cl^--binding site are within ≈3−4 Å of $Y_Z^\bullet$. A model of the active uninhibited OEC could thus be represented by a modification of Figure 4, with chloride replacing the bound acetate. This model shows just one of many possible configurations consistent with the current data, but evidence is clearly building that $Y_Z^\bullet$, the Mn cluster, and Cl^- cofactor are all localized in a compact catalytic unit.

Evidence for Proton Transfer by $Y_Z^\bullet$. The proton/hydrogen atom abstraction models for water oxidation predict decidedly different functions for Y_D and Y_Z. The Y_D tyrosine is oxidized and reduced by the same chlorophyll moiety, P_{680}^+/P_{680} (*63*). During the oxidation, the phenoxy proton is transferred to D2-His189 (*41*), and the proton is transferred back to Y_D upon its reduction (*64*). For this function, Y_D tyrosine needs to undergo hydrogen-bonding interactions with a single proton donor/acceptor (D2-His189, Scheme 1a). This is manifested in the ^2H ESEEM of $Y_D^\bullet$ being well simulated by a single deuteron at a characteristic hydrogen-bonded distance (1.81 Å).

If Y_Z only served as an electron transfer agent, then it would be functionally different from Y_D in that, although it would be oxidized by P_{680}^+, it would be reduced by another species, the Mn cluster. However, there would be no functional need for more than one hydrogen-bonding partner—the proton could shuttle back and forth in the same way as described for the Y_D tyrosine (Scheme 1b).

On the other hand, if $Y_Z^\bullet$ acts to abstract protons or H atoms from substrate water, i.e., Y_Z serves as a proton transfer agent as well as an electron transfer agent, then there will be two separate hydrogen-bonding interaction sites. One site provides for proton donation to $Y_Z^\bullet$ upon the $Y_Z^\bullet \rightarrow Y_Z$ reduction, either directly from substrate water or through a proton transfer intermediate, while the other site accepts protons from Y_Z during the $Y_Z \rightarrow Y_Z^\bullet$ oxidation, as the first step in proton translocation to the lumenal phase (Scheme 1c). Our split-signal ESEEM results, quantifying two deuterons exchanged into sites at hydrogen-bonding distance from the $Y_Z^\bullet$ oxy group, therefore provide strong additional support for the proton/H atom transfer models.

The ESEEM results also provide information about the proton transfer kinetics in the OEC. The split-signal form of $Y_Z^\bullet$ is trapped by freezing illuminated PSII membranes on the time scale of several seconds. Under these conditions, in our model illustrated in Scheme 1c, the ^2H modulation depth indicates that the proton(deuteron) transferred to the acceptor is retained at the site of this proximal base and not transferred away to one or more remote sites. This is consistent with recent results on the P_{680} electrochromism measurements, which have been interpreted to favor charge retention in the OEC (*63*, *65*). However, the electrochromism experiments provide a very indirect measure of charge retention in the OEC, and other interpretations can possibly explain the slow electrochromism relaxation (*66*). We therefore do not consider that our observation of retention of the proton acceptor hydrogen bond in the acetate-treated sample rules out rapid proton transfer to the lumen on the time scale of $Y_Z^\bullet$ oxidation. First, our results are obtained in inhibited PSII samples, and we do not know if the proton is retained in oxygen-evolving preparations. Second, even if the accepted proton is retained, it may be accompanied by injection of a secondary proton into the lumen. For example, such a proton could originate from the distal nitrogen of the histidine H-bond acceptor shown in Scheme 1c.

CONCLUSIONS

The pulsed EPR results obtained in this study of $Y_Z^\bullet$ trapped in the split-signal form in acetate-inhibited PSII membranes lead to a picture of the OEC that locates the tetranuclear Mn cluster, the redox-active tyrosine Y_Z, and the essential cofactor Cl^-, all within a compact unit of a few angstroms extent. Such an OEC geometry is consistent with the proposals that the water-splitting chemistry proceeds through a metalloradical mechanism employing both the Mn cluster and the $Y_Z^\bullet$ neutral radical (*6*, *8*−*10*). The observation that there are two hydrogen bond interactions for $Y_Z^\bullet$ in the trapped $S_2-Y_Z^\bullet$ configuration of the acetate-inhibited PSII sample provides direct spectroscopic support for these recent metalloradical proton/H atom transfer models.

NOTE ADDED IN PROOF

We have recently obtained split-signal EPR spectra of acetate-inhibited PSII membranes oriented on plastic sheets (D. A. Force, K. L. Clemens, K. A. Campbell, D. M. Gingell, and R. D. Britt, unpublished results). Analysis of these new spectra, particularly the spectrum obtained with the membrane normal aligned parallel to the applied magnetic field, shows that the Mn cluster$-Y_Z^\bullet$ magnetic interaction has rhombic symmetry, probably due to the finite size of the Mn cluster and its close proximity to $Y_Z^\bullet$. The simulations displayed in Figure 1 are based on the assumption of an interaction which has an isotropic exchange component and an axial point−dipole component. We are working to simulate both the nonoriented and oriented split-signal spectra using rhombic interactions, and these simulations may lead to a revised estimate of the $Mn-Y_Z^\bullet$ distance.

ACKNOWLEDGMENT

Ribonucleotide reductase samples were kindly provided by Dr. Pamela Riggs-Gelasco and Professor JoAnne Stubbe in the Department of Chemistry of the Massachusetts Institute of Technology.

REFERENCES

1. Babcock, G. T., Barry, B. A., Debus, R. J., Hoganson, C. W., Atamian, M., McIntosh, L., Sithole, I., and Yocum, C. F. (1989) *Biochemistry 28*, 9557−9565.
2. Hansson, Ö., and Wydrzynski, T. (1990) *Photosynth. Res. 23*, 131−162.

[12] Definitive evidence for the exact number and location of Cl^- binding sites in PSII has remained elusive (*3*−*5*). In their most recent work, Lindberg and Andréasson [(1996) *Biochemistry 35*, 14259−14267.] propose a one-site, two-state model for chloride binding in PSII with a low-affinity, rapidly exchanging ($t_{1/2}$ < 15 s) "open conformation" and a high-affinity, slowly exchanging ($t_{1/2}$ = 1 h) "closed conformation", where the rapidly exchanging conformation is induced by Cl^- depletion. In our samples, acetate is introduced following Cl^- depletion and is allowed to incubate for a minimum of 90 min before freezing to 77 K. These conditions should allow for full exchange into the Cl^--competitive site. However, we offer the caveat that even if acetate is competitive with chloride in steady-state measurements, it does not rigorously prove that acetate is bound in the same site in this trapped $S_2 + Y_Z^\bullet$ state that Cl^- would be bound in the physiological S_3 state.

3. Debus, R. J. (1992) *Biochim. Biophys. Acta 1102*, 269−352.
4. Rutherford, A. W., Zimmermann, J.-L., and Boussac, A. (1992) in *The Photosystems: Structure, Function, and Molecular Biology* (Barber, J., Ed.) pp 179−229, Elsevier, Amsterdam.
5. Sauer, K., Yachandra, V. K., Britt, R. D., and Klein, M. P. (1992) in *Manganese Redox Enzymes* (Pecorarro, V. L., Ed.) pp 141−174, VCH, New York.
6. Britt, R. D. (1996) in *Biophysical Techniques in Photosynthesis* (Amesz, A., and Hoff, A. J., Eds.) pp 235−253, Kluwer Academic, Dordrecht, The Netherlands.
7. Kok, B., Forbush, B., and McGloin, P. (1970) *Photochem. Photobiol. 11*, 457−475.
8. Gilchrist, M. L., Ball, J. A., Randall, D. W., and Britt, R. D. (1995) *Proc. Natl. Acad. Sci. U.S.A. 92*, 9545−9549.
9. Hoganson, C. W., Lyadkis-Simantiris, N., Tang, X.-S., Tommos, C., Warncke, K., Babcock, G. T., Diner, B. A., McCracken, J., and Styring, S. (1995) *Photosynth. Res. 46*, 177−184.
10. Tommos, C., Tang, X.-S., Warncke, K., Hoganson, C. W., Styring, S., McCracken, J., Diner, B. A., and Babcock, G. T. (1995) *J. Am. Chem. Soc. 117*, 10325−10335.
11. Tang, X.-S., Randall, D. W., Force, D. A., Diner, B. A., and Britt, R. D. (1996) *J. Am. Chem. Soc. 118*, 7638−7639.
12. Lewis, E. S. (1975) in *Proton-Transfer Reactions* (Caldin, E., and Gold, V., Eds.) pp 317−338, Chapman and Hall, London.
13. Diner, B. A., Force, D. A., Randall, D. W., Chisholm, D. A., Tang, X.-S., and Britt, R. D., unpublished results.
14. Babcock, G. T., Espe, M., Hoganson, C., Lydakis-Simantiris, N., McCracken, J., Shi, W., Styring, S., Tommos, C., and Warncke, K. (1997) *Acta Chem. Scand. 51*, 533−540.
15. Boussac, A., Zimmermann, J.-L., Rutherford, A. W., and Lavergne, J. (1990) *Nature 347*, 303−306.
16. Hallahan, B. J., Nugent, J. H. A., Warden, J. T., and Evans, M. C. W. (1992) *Biochemistry 31*, 4562−4573.
17. Boussac, A., and Rutherford, A. W. (1992) *Biochemistry 31*, 7441−7445.
18. Boussac, A., Zimmermann, J.-L., and Rutherford, A. W. (1989) *Biochemistry 28*, 8984−8989.
19. Sivaraja, M., Tso, J., and Dismukes, G. C. (1989) *Biochemistry 28*, 9459−9464.
20. Boussac, A., Zimmermann, J.-L., and Rutherford, A. W. (1990) *FEBS Lett. 277*, 69−74.
21. Sandusky, P. O., and Yocum, C. F. (1986) *Biochim. Biophys. Acta 849*, 85−93.
22. Sinclair, J. (1984) *Biochim. Biophys. Acta 764*, 247−252.
23. Szalai, V. A., and Brudvig, G. W. (1996) *Biochemistry 35*, 1946−1953.
24. Szalai, V. A., and Brudvig, G. W. (1996) *Biochemistry 35*, 15080−15087.
25. Berthold, D. A., Babcock, G. T., and Yocum, C. F. (1981) *FEBS Lett. 134*, 231−234.
26. Ford, R. C., and Evans, M. C. W. (1983) *FEBS Lett. 160*, 159−164.
27. Kim, D. H., Britt, R. D., Klein, M. P., and Sauer, K. (1992) *Biochemistry 31*, 541−547.
28. MacLachlan, D. J., and Nugent, J. H. A. (1993) *Biochemistry 32*, 9772−9780.
29. Salowe, S. P., and Stubbe, J. (1986) *J. Bacteriol. 165*, 363−366.
30. Bollinger, J. M., Tong, W. H., Ravi, N., Huynh, B. H., Edmondson, D. E., and Stubbe, J. (1994) *J. Am. Chem. Soc. 116*, 8015−8023.
31. Sturgeon, B. E., and Britt, R. D. (1992) *Rev. Sci. Instrum. 63*, 2187−2192.
32. Sturgeon, B. E., Ball, J. A., Randall, D. W., and Britt, R. D. (1994) *J. Phys. Chem. 98*, 12871−12883.
33. Britt, R. D. (1993) *Curr. Opin. Struct. Biol. 3*, 774−779.
34. Mims, W. B., and Peisach, J. (1981) in *Biological Magnetic Resonance* (Berliner, L. J., and Ruben, J., Eds.) pp 213−263, Plenum Press, New York.
35. Mims, W. B., Davis, J. L., and Peisach, J. (1990) *J. Magn. Reson. 86*, 273−292.
36. Mims, W. B. (1984) *J. Magn. Reson. 59*, 291−306.
37. Mims, W. B. (1972) in *Electron Paramagnetic Resonance* (Geschwind, S., Ed.) pp 263−351, Plenum Press, New York.
38. Britt, R. D., Zimmermann, J.-L., Sauer, K., and Klein, M. P. (1989) *J. Am. Chem. Soc. 111*, 3522−3532.
39. Mims, W. B. (1965) *Proc. R. Soc. London, Ser. A 283*, 452−457.
40. Force, D. A., Randall, D. W., Britt, R. D., Tang, X.-S., and Diner, B. A. (1995) *J. Am. Chem. Soc. 117*, 12643−12644.
41. Campbell, K. A., Peloquin, J. M., Diner, B. A., Tang, X.-S., Chisholm, D. A., and Britt, R. D. (1997) *J. Am. Chem. Soc. 119*, 4787−4788.
42. Dole, F., Diner, B. A., Hoganson, C. W., Babcock, G. T., and Britt, R. D. (1997) *J. Am. Chem. Soc.* (in press).
43. Rigby, S. E. J., Nugent, J. H. A., and O'Malley, P. J. (1994) *Biochemistry 33*, 1734−1742.
44. Fan, C. L., Kennedy, M. C., Beinert, H., and Hoffman, B. M. (1992) *J. Am. Chem. Soc. 114*, 374−375.
45. Bender, C. J., Sahlin, M., Babcock, G. T., and Barry, B. A. (1989) *J. Am. Chem. Soc. 111*, 8076−8083.
46. Lai, A., Flanagan, H. L., and Singel, D. J. (1988) *J. Chem. Phys. 89*, 7161−7166.
47. Fiege, R., Zweygart, W., Bittl, R., Adir, N., Genger, G., and Lubitz, W. (1996) *Photosynth. Res. 48*, 227−237.
48. Randall, D. W., Gelasco, A., Caudle, M. T., Pecoraro, V. L., and Britt, R. D. (1997) *J. Am. Chem. Soc. 119*, 4481−4491.
49. Zheng, M., and Dismukes, G. C. (1996) *Inorg. Chem. 35*, 3307−3319.
50. Randall, D. W., Sturgeon, B. E., Ball, J. A., Lorigan, G. A., Chan, M. K., Klein, M. P., Armstrong, W. H., and Britt, R. D. (1995) *J. Am. Chem. Soc. 117*, 11780−11789.
51. Randall, D. W. (1997) Ph.D. Thesis, University of California, Davis.
52. Ono, T., and Inoue, Y. (1990) in *Current Research in Photosynthesis* (Baltscheffsky, M., Ed.) pp 741−744, Kluwer Academic, Dordrecht, The Netherlands.
53. Zimmermann, J.-L., Boussac, A., and Rutherford, A. W. (1993) *Biochemistry 32*, 4831−4891.
54. Lorigan, G. A., and Britt, R. D. (1994) *Biochemistry 33*, 12072−12076.
55. Orbach, R. (1961) *Proc. R. Soc. London, Ser. A 264*, 485−495.
56. Orbach, R. (1961) *Proc. R. Soc. London, Ser. A 264*, 458−484.
57. Hansson, Ö., Aasa, R., and Vänngård, T. (1987) *Biophys. J. 51*, 825−832.
58. Ono, T., Zimmermann, J.-L., Inoue, Y., and Rutherford, A. W. (1986) *Biochim. Biophys. Acta 851*, 193−201.
59. Arnon, D. I., and Tang, G. M.-S. (1988) *Proc. Natl. Acad. Sci. U.S.A. 85*, 9524−9528.
60. Yachandra, V. K., DeRose, V. J., Latimer, M. J., Mukerji, I., Sauer, K., and Klein, M. P. (1993) *Science 260*, 675−679.
61. Wincencjusz, H., van Gorkom, H. J., and Yocum, C. F. (1997) *Biochemistry 36*, 3663−3670.
62. Sandusky, P. O., and Yocum, C. F. (1984) *Biochim. Biophys. Acta 766*, 603−611.
63. Diner, B. A., Tang, X.-S., Zheng, M., Dismukes, G. C., Force, D. A., Randall, D. W., and Britt, R. D. (1995) in *Photosynthesis: From Light into Biosphere* (Mathis, P., Ed.) pp 229−234, Kluwer Academic, Montpellier, France.
64. Diner, B. A., and Babcock, G. T. (1996) in *Oxygenic Photosynthesis: The Light Reactions* (Ort, D. R., and Yocum, C. F., Eds.) pp 213−247, Kluwer Academic, Dordrecht, The Netherlands.
65. Rappaport, F., Blanchard-Desce, M., and Lavergne, J. (1994) *Biochim. Biophys. Acta 1184*, 178−192.
66. Haumann, M., and Junge, W. (1996) in *Oxygenic Photosynthesis: The Light Reactions* (Ort, D. R., and Yocum, C. F., Eds.) pp 165−192, Kluwer Academic, Dordrecht, The Netherlands.

BI9712504